applied sciences

MDPI

Article

Suitability of Dual-Band, Dual-Polarized Patch Antennas with a Superstrate for the Miniaturization of Ku-Band Antenna Arrays for Automotive Applications

Roslin Francis [1,*], Safwat Irteza Butt [1], Jasmeet Singh [1], Peter Guelzow [1], Ralf Eimertenbrink [1] and Matthias A. Hein [2]

[1] Robert Bosch GmbH, 31139 Hildesheim, Germany; safwatirteza.butt@de.bosch.com (S.I.B.); jasmeet.singh@de.bosch.com (J.S.); peter.guelzow@de.bosch.com (P.G.); ralf.eimertenbrink@de.bosch.com (R.E.)
[2] RF & Microwave Research Group, Technische Universität Ilmenau, 98693 Ilmenau, Germany; matthias.hein@tu-ilmenau.de
* Correspondence: roslin.francis@de.bosch.com

Abstract: The extension of low-earth orbit (LEO) services to non-terrestrial mobile communications has huge potential for eliminating network white spots and providing high-speed, low-latency links with worldwide geographic coverage. State-of-the-art user terminals for mobile platforms are too large for integration into a passenger vehicle. Antenna elements loaded with a dielectric superstrate could potentially lead to a considerable miniaturization of the user terminal. As per link budget calculations, an array with a gain of 27 dBi is necessary to ensure a throughput of 25 Mbps in the downlink at the Ku-band. A conventional array with a gain of 6 dBi per element, assuming a 12 × 12 arrangement with half-wavelength spacing, would require a footprint of 36 λ^2 at 10 GHz to achieve this target and appears unsuitable for automotive integration. This paper proposes a low-profile, dual-band, dual-polarized, vertically stacked patch antenna with superstrate loading and shows that the inclusion of the superstrate improves the antenna's gain by at least 3 dB. Therefore, compared to a conventional array, a superstrate-loaded array would need only half of the number of elements to meet the target gain, thus occupying only half of the surface area, and offers better integration for automotive applications. Requiring half of the number of elements also implies considerably reduced design complexity and cost.

Keywords: compact phased array; Ku-band; LEO satellite

Citation: Francis, R.; Butt, S.I.; Singh, J.; Guelzow, P.; Eimertenbrink, R.; Hein, M.A. Suitability of Dual-Band, Dual-Polarized Patch Antennas with a Superstrate for the Miniaturization of Ku-Band Antenna Arrays for Automotive Applications. *Appl. Sci.* **2023**, *13*, 10867. https://doi.org/10.3390/app131910867

Academic Editor: Mario Lucido

Received: 21 August 2023
Revised: 11 September 2023
Accepted: 26 September 2023
Published: 29 September 2023

1. Introduction

The successful implementation of highly automated driving, connected cars (5G/6G), and efficient fleet management demands real-time wireless connectivity architectures with functional redundancy [1]. This is considered a pre-requisite to enable fail-operational automated driving functionality within the operational design domain. Redundant connectivity links are mandatory for such safety-relevant applications, according to current traffic regulations. LEO satellite systems offer non-terrestrial network (NTN) connectivity and can serve as supplements or back-ups for terrestrial networks (TNs) and thus help meet regulatory requirements. The 5G Automotive Association (5GAA) pushes the need for seamless interactions between TNs and NTNs by 2030 [2]. This will be critical for the future car industry so as to ensure continuity of service for mobile users anywhere and at any time. NTNs using suitable LEO satellite constellations promise broadband internet access with latencies below 50 ms and data rates up to hundreds of Mbps, allowing for high-quality multimedia, connectivity, and broadcasting. Moreover, this wireless functionality enables global coverage, especially in remote areas where terrestrial networks are sparse [3]. However, the required link budget of an NTN system, including the transmit power, antenna gain, and frequency bandwidth, in combination with the potentially large

size of the antenna, poses challenges for its integration into a car. As state-of-the-art examples, the Starlink antenna terminal from Space-X [4], Amazon's Ka-band antenna for Kuiper satellites [5], the beam-steering antennas from ALCAN Systems [6], the SOTM terminals from Requtech [7], and Kymeta [8], each have a diameter between 30 and 60 cm, i.e., 10 λ and 20 λ at 10 GHz. The integration of such large antennas into cars is not feasible for mass applications. A trade-off between size and performance needs to be found and thoroughly studied in terms of the link budget required for given use cases and the antenna's radiation characteristics, as well as regulatory aspects and a design for manufacturability. There are Ku-band antenna arrays for LEO connectivity available on the market. But the approach to the miniaturization of such an antenna by designing a single antenna element with high gain per unit area is novel. This miniaturization is critical for an automotive application in which space and aesthetics are major constraints. In this regard, this paper proposes a low-profile, dual-band, dual-polarized, vertically stacked patch antenna with a superstrate with a focus on two main aspects:

- The calculation of the LEO satellite link budget, which establishes a general relationship between any desired data rate in downlink and the corresponding antenna gain necessary for achieving the same. Several other authors [9–11] discuss Ku-band antennas (with frequency range of 12 to 18 GHz and wavelengths of 1.7 to 2.5 cm) and the corresponding link budgets. In this paper, the link budget for broadband internet data rates DR >25 Mbps are consolidated for LEO connectivity in Section 2.
- The simulation and measurement results for the proposed single antenna element with and without superstrate loading are presented and discussed. With the superstrate, the single-element gain was enhanced by more than 3 dB, which has significant consequences for the potential miniaturization of the Ku-band array antenna in that theoretically, the array size could be halved compared to an array without superstrate loading. These results are elucidated in Section 3. Section 4 presents the conclusion and the future work.

2. Antenna Array Specifications Based on Link Budget for LEO Connectivity

The aim of this study is to design an antenna capable of delivering broadband internet access which, according to the U.S. Federal Communication Commission (FCC)'s definition, is DR_{DL} = 25 Mbps for download and $DR_{UL} \geq 3$ Mbps for upload [12]. The antenna gain G needed to meet this target is derived from the carrier-to-noise ratio (C/N) at the receiver input. The C/N is represented by Equation (1) [13] and depends on the chosen modulation and coding scheme, channel bandwidth (CBW), and the desired data rate (DR).

$$\left[\frac{C}{N}\right]_{dB} = \frac{E_b}{N_0} + CBW - DR \quad (1)$$

Typical satellite communications use digital video broadcast (DVB-S2) standards for broadcast, and this is assumed as the communication standard for LEO connectivity in this section. There are several modulation and coding schemes available for DVB-S2 systems, and the most common, 16 APSK 2/3, is considered based on the specifications of existing modems available for the application [14–16]. This scheme requires an energy per bit of E_b/N_0 = 4.76 dB [17]. The channel bandwidth is taken to be CBW = 10 MHz. Substituting these values into Equation (1), we obtain C/N = 8.74 dB. This C/N value can be used to calculate the required antenna quality factor G/T as per the link budget in Equation (2) [17].

$$\left[\frac{G}{T}\right]_{dB} = FSPL + L_{atm} + K + RBW - EIRP - \frac{C}{N} \quad (2)$$

Table 1 lists the parameters involved in the calculation of the link budget. The dominant contribution is the free-space path loss ($FSPL$), which depends on the orbital distance d and the frequency f of the signal. The values for d and the satellite's effective isotropic radiated power ($EIRP$) in Table 1 are derived from the specifications of the three major LEO

constellations, namely SpaceX, OneWeb, and Telesat [16]. Further significant contributions result from atmospheric losses (L_{atm}) and the system's noise temperature (T_{sys}). As the Ku-band frequencies are in a range at f > 10 GHz, they are subject to attenuation due to atmospheric effects like cloud, rain, fog, and atmospheric gases, which are accumulated in L_{atm} [17]. The link should be established even under heavy-rain conditions; in other words, at 99.99% availability. Accordingly, a value of L_{atm} = 5 dB [18] was chosen. For an antenna looking at a cold sky during satellite reception, the antenna noise temperature was set to T_{ant} = 20 K [19].

Table 1. Link budget calculations in the Ku-band (downlink).

Parameter	Symbol	Value	Unit
E_b/N_0 required for 16 APSK 2/3	E_b/N_0	4.76	dB
Data rate required	DR	25	Mbps
Channel BW	CBW	10	MHz
Receiver noise BW	RBW	36	MHz
Carrier-to-noise ratio required	C/N	8.74	dB
Carrier-to-noise density required	C/N_0	84.3	dB
Satellite EIRP	$EIRP$	34.6	dBW
Downlink frequency	f_d	12.6	GHz
Path distance	d	1200	km
Free-space path loss	$FSPL$	176.09	dB
Atmospheric losses	L_{atm}	5.0	dB
System noise temperature	T_{sys}	314	K
Roll-off factor	f_{ro}	0.1	
Antenna quality factor required	G/T_{sys}	−2.31	dB/K
Realized gain required	G	27.4	dB

The other contributions are calculated from the noise figure of the RF chain based on typical frontend IC specifications [20]. For a noise figure of F = 3 dB, the effective noise temperature, as per Equation (3), [18] results in T_{FE} = 294 K.

$$T_{FE} = 295 \cdot \left(10^{\frac{F}{10}} - 1\right) \tag{3}$$

Combining these temperatures as per Equation (4) [18] results in T_{sys} = 314 K as the system noise temperature.

$$T_{sys} = T_{ant} + T_{FE} \tag{4}$$

Substituting this value in Equation (2) and additionally taking into account the scan loss through the roll-off factor f_{ro} = 0.1 [16] yields the required realized gain, G = 27.4 dBi.

The downlink gain and data rate scale with the number of antenna elements, as summarized in Figure 1, assuming that a single patch antenna provides a realized gain of G_{SE} = 6 dBi. In a dual-band (uplink + downlink) antenna design, the number of antenna elements needed in an array is determined by the higher of the uplink/downlink data rate requirements. As DR_{DL} = 25 Mbps is needed in the downlink but only DR_{UL} = 3 Mbps is needed in the uplink, fulfilling the downlink data rate requirement would automatically satisfy the uplink requirements. This, however, corresponds to an array with 12 × 12 = 144 antenna elements and for the half-wavelength element distance, a footprint of 6 λ × 6 λ = 36 λ^2, which would be too large for automotive applications.

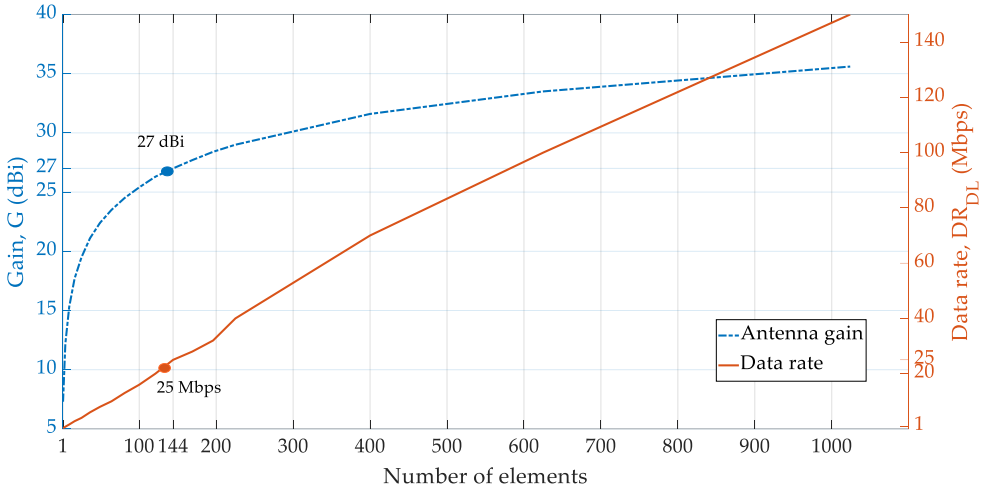

Figure 1. Number of elements required for an antenna array to fulfill the gain and data rate requirements in downlink.

3. Proposed Antenna

Satellite communications predominantly use circularly polarized signals; hence, the proposed antenna is designed to work circularly polarized. Some beamforming integrated circuits combine vertical and horizontal polarizations to form circularly polarized signals via appropriate superposition [21], while other solutions accept circularly polarized signals [22] from the antenna. Here, we decided to design a dual-band, dual-linearly polarized antenna; an ideal quadrature coupler is used in post-processing to obtain circular polarization. The dual band covers downlink (DL) frequencies from 10.8 to 12.6 GHz and uplink (UL) frequencies from 14 to 14.5 GHz. Since there are no existing compact antenna designs for LEO satellite connectivity in automotive applications to the best knowledge of the author, a comparison to other approaches is not presented.

3.1. Design

The use of a microstrip patch appeared to be the most attractive option to achieve a low profile and reduced complexity and cost. Alternative types of antennas would increase the cost and/or complexity. A dipole antenna, for example, would additionally require a balun for mode transformation from a differential feed to an unsymmetric microstrip line, and it would also need to be $\lambda/4$ apart from the underlying ground plane for constructive interference with the ground. As a second example, although it offers a high gain, an array design based on leaky-wave antennas fed via a slotted waveguide [23] would result in a bulky structure and pose limitations on the antenna's beam-steering capabilities.

The single element was designed using electromagnetic full-wave simulations in CST microwave studio [24], with the dimensions mentioned in Figure 2a,b. In this paper, [25] was taken as the starting point for the design of the antenna. Significant changes were made in order to adapt it to our intended application; for example, the feeding structures were optimized, a vertically stacked parasitic patch was included to enhance the impedance bandwidth in addition to other bandwidth-enhancing techniques, as mentioned later, and a low-loss substrate, a Rogers RO4350B (ε_r = 3.66, $tan\delta$ = 0.0037 at 10 GHz) [26], which is suited for high frequencies, was chosen. The feeding was accomplished via aperture coupling, using two microstrip lines that coupled to the two orthogonal H-shaped slots in the antenna ground, exciting dual polarization. In comparison to other techniques like microstrip line feeding, proximity coupling, et cetera, aperture coupling offers the widest bandwidth [27,28].

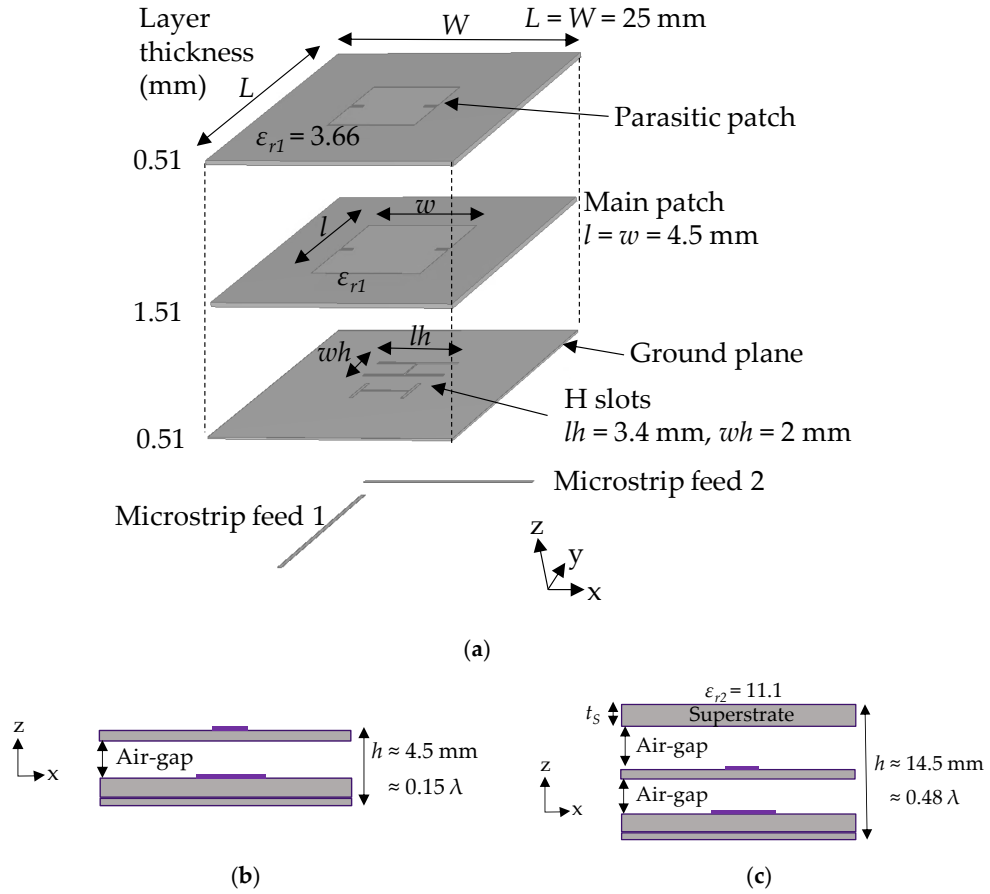

Figure 2. (**a**) Exploded view of the single antenna element; (**b**) side-view; (**c**) side-view of the single antenna element with the superstrate.

The antenna described above would offer a typical single-element realized gain G_{SE} ≈ 6 dBi, but if we would like to create an array with a reduced size, this value should be increased without compromising the surface area, i.e., a higher gain per unit area should be realized. A highly efficient way to achieve this was proposed in [29] and is based on the suspension of a superstrate above a patch antenna. When a relatively large-sized superstrate (>λ) is used over a small radiator with a large ground plane, significant gain enhancement is achievable when the superstrate is suspended at approximately a half-wavelength above the antenna ground. Therefore, in the second step, a superstrate was added which is approximately six times the size of the main patch, as shown in Figure 2c. The superstrate was separated from the parasitic patch by an air gap of 0.27 λ, corresponding to a distance of 8.1 mm at a reference frequency of f = 10 GHz. It has a relative permittivity and loss tangent of ε_r = 11.1 and $tan\delta$ = 0.0022 at 10 GHz. The thickness t_S of the superstrate was 2.5 mm, which is around 0.08 λ. These values were determined through the parametric optimization of the gain achievable at the frequencies of interest.

3.2. Measurement Results with and without the Superstrate

The antenna was manufactured and assembled as in Figure 3a and set up in a shielded anechoic chamber, as shown in Figure 3b, for measurements. Figure 4 compares the measured and simulated S-parameters for the single element without the superstrate. Since the S-parameters of the design with the superstrate were very similar, in accordance with expectations, they were omitted for clarity. The measured $|S_{22}|^2$ *(f)* -curves in the DL band were shifted by 500 MHz to lower the frequencies compared to the simulations, whereas the simulated and measured $|S_{11}|^2$ *(f)*-data follow similar trends. In general, these differences are due to the differences between the idealized and real en-

vironments, for example, the simulations were performed in a free-space environment which did not take into account the presence of antenna probes and positioning equipment. There are also the manufacturing and assembly tolerances of the antenna's geometry and the substrate's properties. The shift in the $|S_{22}|^2$ *(f)* -curves does not, however, influence the measured gain to the extent that the data rate and gain bandwidth are affected. The transmission coefficient was $|S_{12}|^2 < -20$ dB over the entire frequency range, which is in good agreement with the numerical simulations and indicative of good port isolation. The fractional bandwidth requirements of 15 % in downlink and 4% in uplink for LEO satellite connectivity were fulfilled and validated by the measurements.

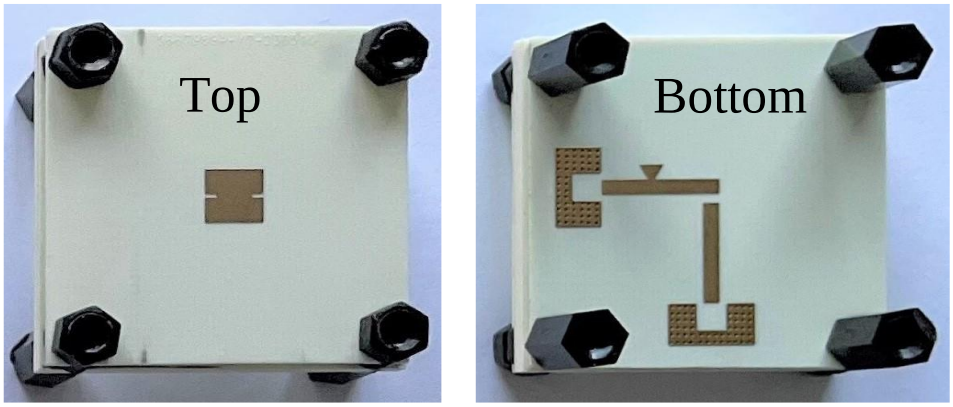

(**a**)

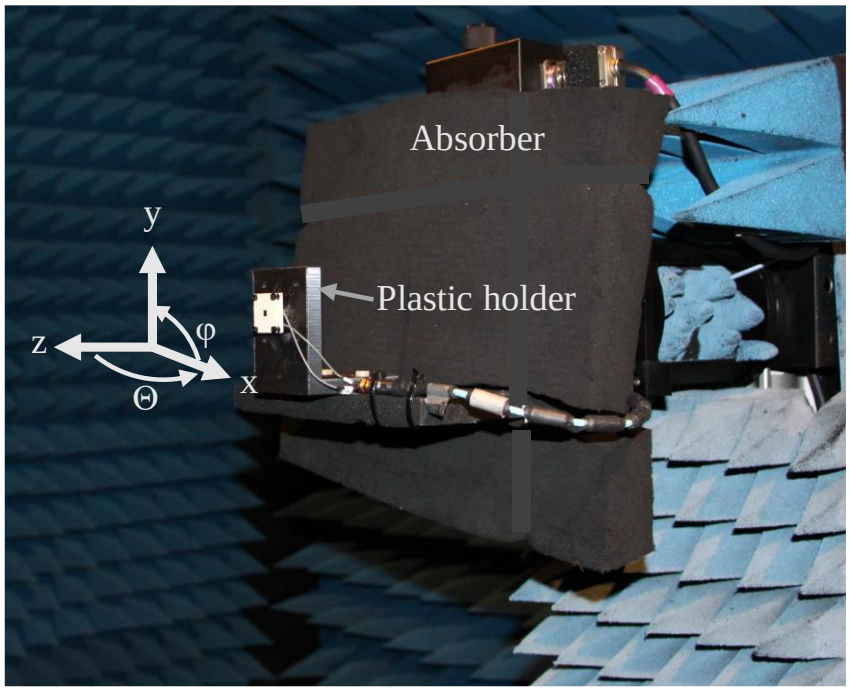

(**b**)

Figure 3. (**a**) Assembly of the single antenna element; (**b**) setup of the antenna for spherical far-field measurements in the shielded anechoic chamber at TU Ilmenau.

From the measured gain curves in Figure 5a, it is clearly visible that the superstrate yields a 3 . . . 6 dB gain improvement across the entire DL-band. There is, however, a shift in the measured gain enhancement compared to the simulations. This shift is attributed to the variations in the dielectric permittivity of the inhomogeneous medium comprised of the air gap and the superstrate; as for the experiments, the superstrate was fixed using four screws above the antenna element. For the final application, these manufacturing anomalies need

to be compensated for to achieve a properly matched antenna. While the improvement in the UL-band was around 2 dB, this is still quite an acceptable performance in view of the significantly relaxed data rate requirement for uplink compared to downlink.

Moving on to Figure 5b,c, the polarization purity was studied by comparing the right-hand circularly polarized (RHCP) and left-hand circularly polarized (LHCP) gain values and the axial ratio (AR) of the main beam at boresight. Over the frequency bands of interest, the RHCP gain was higher than the LHCP gain by 8 . . . 10 dB, and the measured axial ratio was below 5 dB. The lower axial ratio value observed in the measurements compared to the simulated data is the result of shadowing from the positioner. This leads to a weakening of the LHCP beam with respect to the RHCP beam in the boresight.

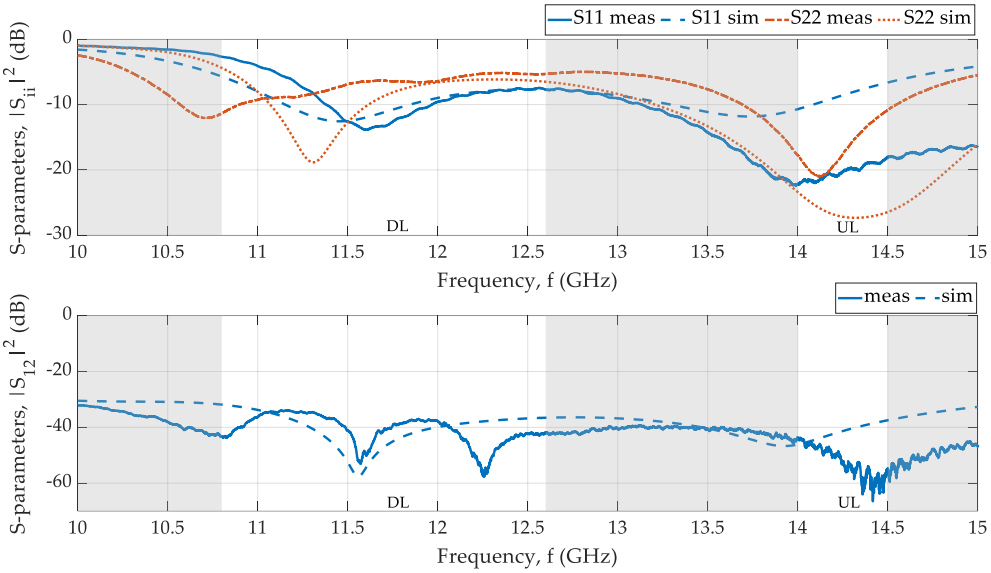

Figure 4. Reflection and transmission coefficients of the single antenna element for input and output matching (top) and isolation (bottom).

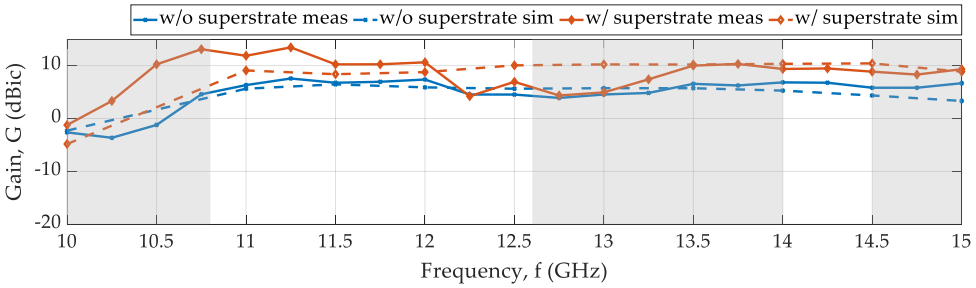

(a)

Figure 5. *Cont.*

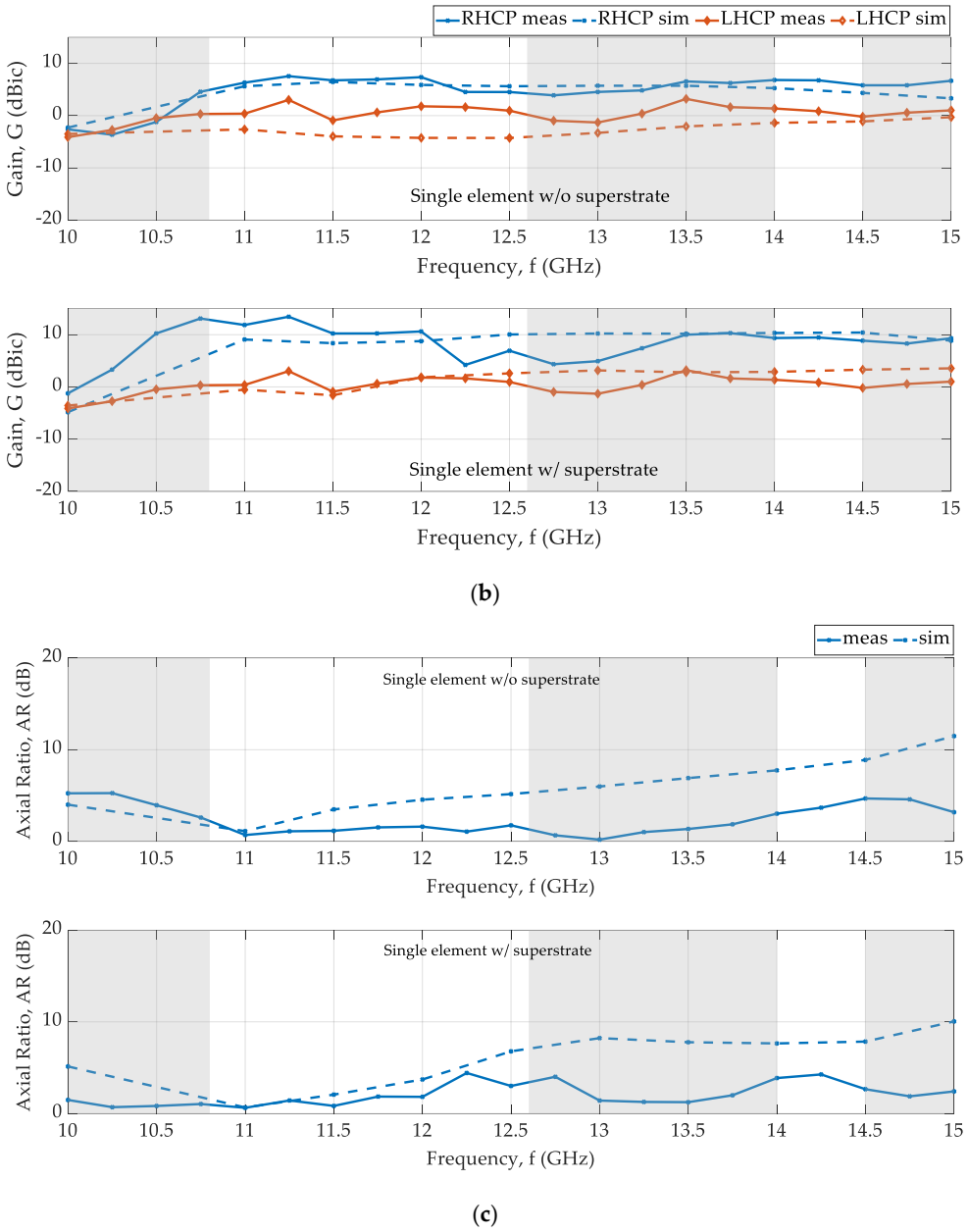

Figure 5. (**a**) Comparison of RHCP gain over frequency in measurements (solid curves) and simulation (dashed curves) without superstrate (blue colour) and with superstrate (orange colour). (**b**) Comparison of RHCP (blue colour) and LHCP gains (orange colour) in simulations (dashed curves) and measurements (solid curves) without superstrate (top) and with superstrate (bottom). (**c**) Comparison of axial ratio over frequency in simulations (dashed curves) and measurements (solid curves) without superstrate (top) and with superstrate (bottom).

In Figure 6a–d, the elevation cuts of the normalized RHCP gain are plotted for the downlink frequency f = 11 GHz and show very good agreement between the simulations and the measurements. The antenna performance at the uplink frequency f = 14 GHz is presented in Figure 7a–d. The normalized cuts of the measured and simulated RHCP patterns are comparable for the case without the superstrate, while the measurement with the superstrate deviates from the simulation, as seen in Figure 7b, especially the appearance of the null, which is not observed in the simulations. This null in the measurements can be attributed to the artifacts in the measurement setup and requires further investigation.

Such a null in the application can be detrimental for reception quality; however, in the phased array design, the null can be compensated for using adaptive weighting algorithms.

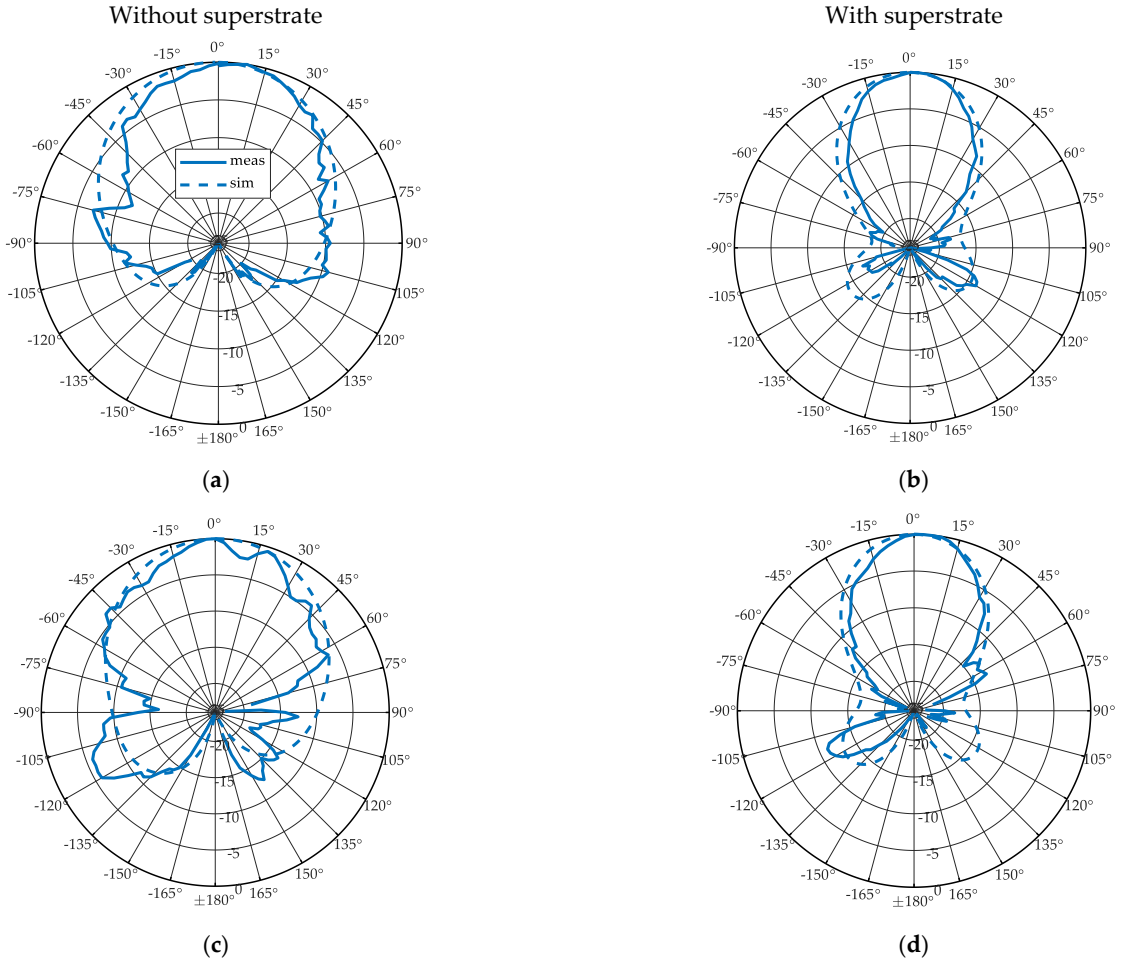

Figure 6. Normalized elevation cuts for the single element at 11 GHz in the measurements (solid curves) and simulation (dashed curves) without the superstrate (left) and with the superstrate (right) for (**a**) Elevation cut Φ = 0°, (**b**) Elevation cut Φ = 0°, (**c**) Elevation cut Φ = 90°, and (**d**) Elevation cut Φ = 90°.

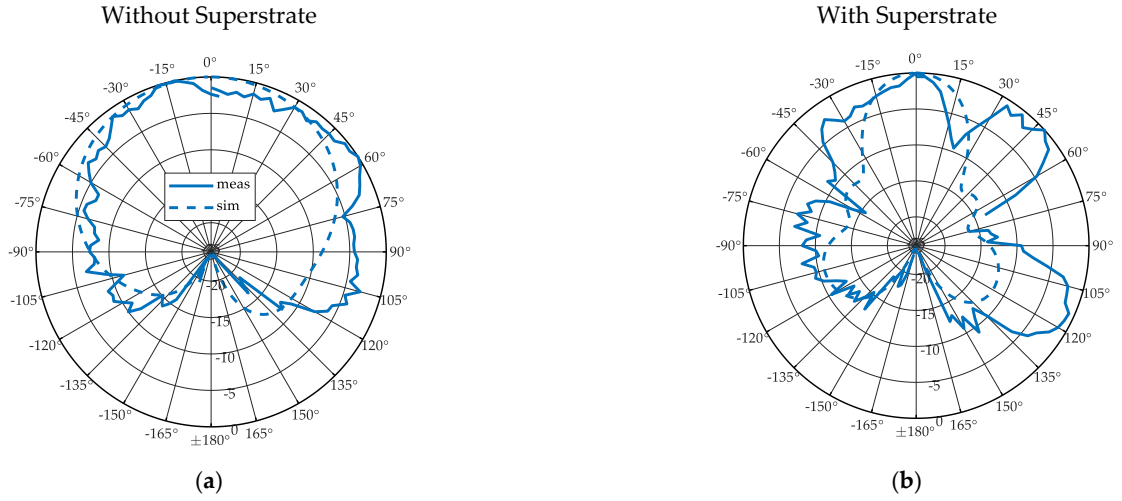

Figure 7. *Cont.*

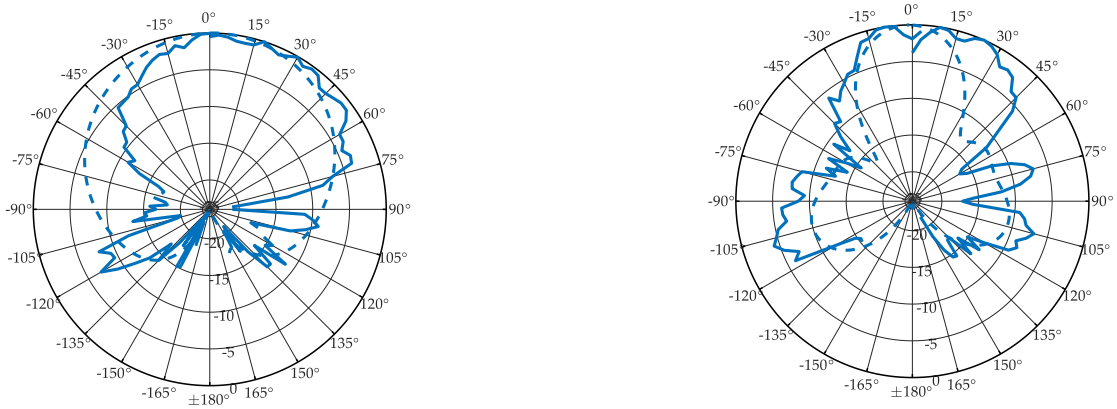

Figure 7. Normalized elevation cuts for the single element at 14 GHz in the measurements (solid curves) and simulation (dashed curves) without the superstrate (left) and with the superstrate (right) for (**a**) Elevation cut Φ = 0°, (**b**) Elevation cut Φ = 0°, (**c**) Elevation cut Φ = 90°, and (**d**) Elevation cut Φ = 90°.

The key parameters corresponding to Figures 6 and 7 are presented in Table 2. The total efficiency (η) for each frequency was calculated by substituting the values of the maximum RHCP realized gain $G_{max}(\theta,\Phi)$ and the respective maximum directivity $D_{max}(\theta,\Phi)$ in Equation (5) [30]. At 14 GHz, the measured efficiency with the superstrate was around 40% lower than the simulated efficiency as the measured directivity was approximately 3 dB higher for similar realized gains in the simulations and measurements.

$$\eta = \frac{G_{max}(\theta,\Phi)}{D_{max}(\theta,\Phi)} \tag{5}$$

Table 2. Simulated and measured antenna characteristics with and without the superstrate at 11 and 14 GHz.

Parameter	11 GHz			
	Without Superstrate		**With Superstrate**	
	Simulated	**Measured**	**Simulated**	**Measured**
Gmax(θ,Φ) (dBic)	5.6	6.3	9	11.8
η (%)	77	85	89	97
FBR (dB)	29	42	34	37
HPBW, Φ = 0° (°)	77	63	47	42
HPBW, Φ = 90° (°)	77	50	48	42
	14 GHz			
Gmax(θ,Φ) (dBic)	5.28	6.8	10.35	9.4
η (%)	88	76	89	55
FBR (dB)	26	40	27	25
HPBW, Φ = 0° (°)	112	114	33	20
HPBW, Φ = 90° (°)	94	80	32	60

The value of $D_{max}(\theta,\Phi)$ in Equation (5) was obtained by taking the ratio of the maximum radiated power of the antenna to the power averaged at all azimuth (Φ) and elevation (θ) angles around the antenna at that particular frequency, as shown in Equation (6) [29].

$$D_{max}(\theta,\Phi) = \frac{4\pi\ P_{max}(\theta,\Phi)}{\Sigma P_{max}(\theta,\Phi)} \tag{6}$$

The front-to-back ratio (*FBR*) mentioned in Table 2 is based on the power ratio of the beam from θ = 0° to θ = 180°, and the half-power beamwidth (*HPBW*) is based on the

elevation cuts at $\Phi = 0^\circ$ and $\Phi = 90^\circ$. In general, there is a good correlation between the experimental and simulation results in this case.

4. Conclusions

As LEO satellites are a promising solution that can offer higher data rates at very low latencies, they can be used to complement TN and assure seamless connectivity. In order to design an antenna for this application in a passenger car, a link budget analysis was performed. To obtain downlink data rates of 25 Mbps from the link budget, it was concluded that the antenna requires a realized gain of 27 dBi. This means that if each antenna element had a gain of 6 dBi, an array of 12×12 elements would be needed to achieve 27 dBi. This implies a footprint of $6\lambda \times 6\lambda$ with respect to a frequency of 10 GHz or 18×18 cm. Since size is a major constraint for integrating an antenna into the roof of a car, the aim was to design an antenna element that could provide a gain higher than the conventional design. Therefore, a design based on superstrate loading was used to enhance the gain. The antenna was manufactured, assembled, and tested in a shielded anechoic chamber. In the DL-band, measurements showed that there was a 500 MHz shift to a lower frequency in the S11 matching from the simulations. This was due to the difference in the measurement environment and variations in the substrate's properties. The presented antenna design and results show that the inclusion of a superstrate in the single element enhances its realized gain by 3 ... 6 dB. Therefore, this approach looks promising for the miniaturization of a Ku-band antenna array as we could potentially use half of the number of elements using superstrate loading. This could drastically reduce the array size, making it suitable for automotive applications. The reduced number of elements leads to fewer front ends or beamforming integrated circuits which, in turn, reduces cost and manufacturing complexity. Contrary to the size reduction and high gain, the superstrate poses the challenges of scanning range, side-lobe levels, and bandwidth in particular. For applications in which a full-hemisphere beam steering is required, this approach may not be feasible. Similarly, for large fractional bandwidth requirements, the superstrate-based antenna design presents challenges in implementation. These characteristics require further study to define the boundary conditions and constraints for the use of a superstrate in high-gain-antenna array designs.

The following topics are considered for further investigation:

- The behavior of a superstrate integrated into a 2×2 phased array, especially with respect to an analysis of its impact on beam steering. In the measurements, a null was observed in the UL-band for an elevation cut of $\Phi = 0^\circ$. It needs to be determined whether this is caused by the superstrate itself or from measurement artifacts. In order to steer the beam to $\pm 50^\circ$ for satellite tracking, such a null would be detrimental to receiving or transmitting the signal as it can cause interferences.
- The dimension of the superstrate is critical for achieving the maximum gain and for achieving a consistent radiation pattern over the frequency range of interest. Properties such as the dielectric constant, thickness, size, and height of superstrate also play a role in gain enhancement. Therefore, they need to be carefully chosen to attain the best advantage in automotive applications. In the antenna, an increased height and multiple layers lead to additional costs which also need to be studied to reach a compromise between performance, size, and cost.

Author Contributions: Conceptualization, R.F. and S.I.B.; formal analysis, R.F.; resources, P.G. and R.E.; writing – original draft, R.F.; writing—review & editing, S.I.B., J.S. and M.H; Supervision, M.A.H. All authors have read and agreed to the published version of the manuscript.

Funding: This research received no external funding.

Institutional Review Board Statement: Not applicable.

Informed Consent Statement: Not applicable.

Data Availability Statement: Not applicable.

Acknowledgments: The research for this paper was supported by Robert Bosch GmbH in co-operation with RF and Microwave Research Group, TU Ilmenau. The authors would also like to thank Michael Huhn for his valuable technical support in the antenna measurement lab, TU Ilmenau.

Conflicts of Interest: The authors declare no conflict of interest.

References

1. Yastrebova, A.; Ojanperä, T.; Mäkelä, J.; Höyhtyä, M. Hybrid Connectivity for Autonomous Vehicles: Conceptual View & Initial Results. In Proceedings of the 2021 IEEE 93rd Vehicular Technology Conference (VTC2021-Spring), Helsinki, FL, USA, 25–28 April 2021; pp. 1–6. Available online: https://ieeexplore.ieee.org/abstract/document/9448866 (accessed on 28 July 2023).
2. 5GAA Position on the Secure Space-Based Connectivity Programme and Focus on the European Communication Satellite Constellation. Available online: https://5gaa.org/content/uploads/2022/10/5GAA_NTN_Position_Paper.pdf (accessed on 28 July 2023).
3. Yaacoub, E.; Alouini, M.-S. A Key 6G Challenge and Opportunity—Connecting the Base of the Pyramid: A Survey on Rural Connectivity. *Proc. IEEE* **2020**, *108*, 533–582. Available online: https://ieeexplore.ieee.org/document/9042251 (accessed on 28 July 2023). [CrossRef]
4. Starlink Phased Array Antenna. Available online: https://www.starlink.com/specifications (accessed on 28 July 2023).
5. Amazon's Project Kuiper Unveils Three Customer Terminals and Custom Chip. Available online: https://www.edgeir.com/amazons-project-kuiper-unveils-three-customer-terminals-and-custom-chip-20230316 (accessed on 28 July 2023).
6. ALCAN Announces Electronic Beam Steering Ground Antenna for LEO and MEO Satellite Service Use at a Low Price of EUR 1500. Available online: https://www.alcansystems.com/press-release-ngso-ground-antenna/ (accessed on 28 July 2023).
7. Requtech Electronically Scanned Antenna Fully Integrated Satellite Terminal. Available online: https://requtech.com/products/resa-s/ (accessed on 28 July 2023).
8. Kymeta Hawk u8–LEO. Available online: https://www.kymetacorp.com/solutions/hawk-u8-leo/ (accessed on 28 July 2023).
9. Ding, Y.R.; Cheng, Y.J. Ku/Ka Wide-Band Dual-Band Dual-Polarized Shared-Aperture Phased Array Antenna with High Aperture Efficiency. In Proceedings of the 2021 IEEE International Symposium on Antennas and Propagation and USNC-URSI Radio Science Meeting (APS/URSI), Singapore, 4–10 December 2021; pp. 1189–1190. Available online: https://ieeexplore.ieee.org/document/9703882 (accessed on 28 July 2023).
10. Gültepe, G.; Kanar, T.; Zihir, S.; Rebeiz, G.M. A 1024-Element Ku-Band SATCOM Phased-Array Transmitter with 45-dBW Single-Polarization EIRP. *IEEE Trans. Microw. Theory Tech.* **2021**, *69*, 4157–4168. Available online: https://ieeexplore.ieee.org/document/9426952 (accessed on 28 July 2023). [CrossRef]
11. Khan, M.; Yang, Z.; Warnick, K. Dual-Circular-Polarized High-Efficiency Antenna for Ku-Band Satellite Communication. *IEEE Antennas Wirel. Propag. Lett.* **2014**, *13*, 1624–1627. Available online: https://ieeexplore.ieee.org/document/6873213 (accessed on 28 July 2023). [CrossRef]
12. How Fast is Broadband? Available online: https://broadbandusa.ntia.doc.gov/about-us/frequently-asked-questions/how-fast-broadband (accessed on 28 July 2023).
13. Singh, K.; Nirmal, A.V.; Sharma, S.V. Link Margin for Wireless Radio Communication Link. *ICTACT J. Commun. Technol.* **2017**, *8*, 8. Available online: https://www.researchgate.net/publication/320465087_LINK_MARGIN_FOR_WIRELESS_RADIO_COMMUNICATION_LINK/citation/download (accessed on 11 September 2023). [CrossRef]
14. AYECKA Gateway and Modem Solution for LEO. Available online: https://www.ayecka.com/leo (accessed on 28 July 2023).
15. SatixFy SCPC Modem. Available online: https://www.satixfy.com/wp-content/uploads/2020/01/satixfy_brochure_SCPC_A4_NEW2019_Final.pdf (accessed on 28 July 2023).
16. Del Portillo, I.; Cameron, B.G.; Crawley, E.F. A technical comparison of three low earth orbit satellite constellation systems to provide global broadband. *Acta Astronaut.* **2019**, *159*, 123–135. Available online: https://www.sciencedirect.com/science/article/pii/S0094576518320368 (accessed on 28 July 2023). [CrossRef]
17. ETSI EN 302 307 V1.2.1 (2009-08). Available online: https://www.etsi.org/deliver/etsi_en/302300_302399/302307/01.02.01_60/en_302307v010201p.pdf (accessed on 28 July 2023).
18. Daniel, R. Glover, Satellite Radio Communications Fundamentals and Link Budgets. Available online: https://link.springer.com/content/pdf/10.1007/978-1-4419-7671-0_17.pdf (accessed on 28 July 2023).
19. Gültepe, G.; Kanar, T.; Zihir, S.; Rebeiz, G.M. A 1024-Element Ku-Band SATCOM Dual-Polarized Receiver with >10-dB/K G/T and Embedded Transmit Rejection Filter. *IEEE Trans. Microw. Theory Tech.* **2021**, *69*, 3484–3495. Available online: https://ieeexplore.ieee.org/document/9416306 (accessed on 28 July 2023). [CrossRef]
20. ADTR1107 6 GHz to 18 GHz, Front-End IC. Available online: https://www.analog.com/en/products/adtr1107.html#product-overview (accessed on 28 July 2023).
21. F6121, 16-Channel Dual-beam Rx Active Beamforming IC, Ku-Band SATCOM. Available online: https://www.renesas.com/us/en/products/rf-products/phased-array-beamformers/f6121-16-channel-dual-beam-rx-active-beamforming-ic-ku-band-satcom?gclid=EAIaIQobChMI16OZrYasgAMVcJCDBx1_9Q1cEAAYASAAEgIn2vD_BwE (accessed on 28 July 2023).
22. ADAR1000 8 GHz to 16 GHz, 4-Channel, X Band, Ku Band Beamformer. Available online: https://www.analog.com/en/products/adar1000.html (accessed on 28 July 2023).

23. Krauss, A.; Bayer, H.; Stephan, R.; Hein, M. Low-Profile Tracking Antenna for Ka-Band Satellite Communications. 207–210. 2013. Available online: https://www.researchgate.net/publication/261038454_Low-profile_tracking_antenna_for_Ka-band_satellite_communications (accessed on 28 July 2023).
24. CST Studio Suite. Available online: https://www.3ds.com/de/produkte-und-services/simulia/produkte/cst-studio-suite/ (accessed on 28 July 2023).
25. Chiou, T.-W.; Wong, K.-L. A Compact Dual-Polarized Aperture-Coupled Patch Antenna for GSM 900/1800-MHz Systems. APMC 2001. In Proceedings of the 2001 Asia-Pacific Microwave Conference (Cat. No.01TH8577), Taipei, Taiwan, 3–6 December 2001; Volume 1, pp. 95–98. Available online: https://ieeexplore.ieee.org/abstract/document/985597 (accessed on 28 July 2023).
26. RO4000®Series High Frequency Circuit Materials. Available online: https://www.rogerscorp.com/-/media/project/rogerscorp/documents/advanced-electronics-solutions/english/data-sheets/ro4000-laminates-ro4003c-and-ro4350b{-}{-}-data-sheet.pdf (accessed on 28 July 2023).
27. A Review of Aperture Coupled Microstrip Antennas: History, Operation, Development, and Applications. Available online: https://people.umass.edu/dpozar/miscfiles/aperture.pdf (accessed on 28 July 2023).
28. Design of Wideband Circularly Polarized Aperture-Coupled Microstrip Antennas. Available online: https://ieeexplore.ieee.org/stamp/stamp.jsp?arnumber=214613 (accessed on 28 July 2023).
29. Yu, Y.-H.; Zong, Z.-Y.; Wu, W.; Fang, D.-G. Dielectric Slab Superstrate Electrically Small Antennas with High Gain and Wide Band. *IEEE Antennas Wirel. Propag. Lett.* **2020**, *19*, 1476–1480. Available online: https://ieeexplore.ieee.org/document/9128031 (accessed on 28 July 2023). [CrossRef]
30. Balanis, C.A. *Antenna Theory Analysis and Design*, 3rd ed.; John Wiley & Sons: Hoboken, NJ, USA, 2005.